Available online at www.sciencedirect.com
SCIENCE DIRECT®
Journal of Magnetic Resonance 170 (2004) 177–183
JMR Journal of Magnetic Resonance
www.elsevier.com/locate/jmr

Single point imaging with suppressed sound pressure levels through gradient-shape adjustment

Peter Latta[a,b,*], Marco L.H. Gruwel[a], Earle Edie[a], Miloš Šrámek[c], Boguslaw Tomanek[a]

[a] Institute for Biodiagnostics, National Research Council of Canada, 435 Ellice Avenue, Winnipeg, Manitoba, Canada R3B 1Y6
[b] Institute of Measurement Science, Slovak Academy of Sciences, Dúbravská cesta 9, SK-84219 Bratislava, Slovakia
[c] OAW—Visualisierung Donau-City-Strasse 1 A-1220 Vienna, Austria

Received 7 April 2004; revised 21 June 2004
Available online 23 July 2004

Abstract

Acoustic noise produced during single point imaging (SPI) experiments was modulated by changes in the spatial encoding gradients. Parameters of both linear and sine-shaped gradient ramps were modified to minimize the acoustic noise levels. Acoustic noise measurements during SPI were measured on three different gradient systems and revealed that for small gradient-bore systems a considerable acoustic noise reduction of more than 20 dB can easily be achieved. SPI in conjunction with an optimized gradient waveform can be a superb alternative to the previously introduced single point ramped imaging with T_1 enhancement (SPRITE) method when sound levels and overheating of gradients are a concern.

Keywords: Magnetic resonance imaging; Single point imaging; Gradient; Acoustic noise

1. Introduction

The single point imaging (SPI) method, originally introduced by Emid and Creyghton [1], has already proven its potential for the imaging of solids, semi-solids, and other broad-line samples with very short transverse relaxation times. Several applications of SPI have been reported for imaging of solid materials [2] and biological samples [3].

SPI uses phase encoding for all spatial dimensions and during each repetition of the experiment only one point in k-space is sampled. Accordingly, the gradient program is very simple. Once gradients have reached their final, stable amplitude, a radiofrequency (RF) pulse is applied and a single data point is acquired after which the gradients are turned off (see Fig. 1). There is no need for time consuming gradient switching, as is often the case in other standard NMR imaging methods. This means that SPI allows for rapid NMR signal acquisition (one point for each phase encoding step); typically acquisition occurs 50–400 μs after excitation of the spin system. For samples with very short T_2 relaxation times this is very important in order to obtain signal before spin–spin relaxation has destroyed the FID. As SPI is a pure phase encoding technique, B_0 inhomogeneity and chemical shift artifacts do not affect the final images. On the other hand, the phase encoding of all spatial directions makes SPI time inefficient compared to conventional imaging techniques, which use a combination of phase and frequency encoding of k-space. However, this is usually partially compensated for by a short T_1 relaxation time of the samples. A short T_1 allows for a short repetition time (T_R) in the SPI sequence, typically on the order of 1–10 ms. Recently, to make data acquisition more efficient and faster, the original SPI sequence

* Corresponding author. Fax: +1-204-984-7036.
E-mail address: peter.latta@nrc-cnrc.gc.ca (P. Latta).

1090-7807/$ - see front matter © 2004 Elsevier Inc. All rights reserved.
doi:10.1016/j.jmr.2004.06.012

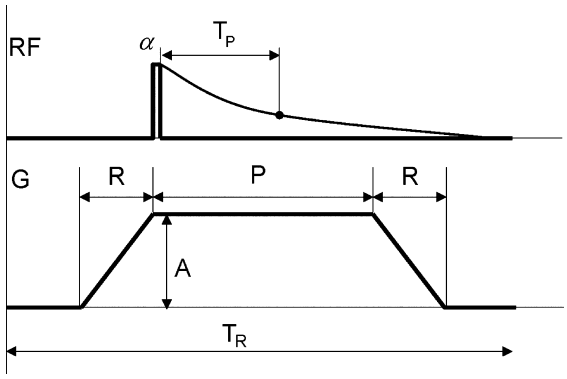

Fig. 1. SPI pulse sequence diagram (only one phase encoding dimension is show). The transverse magnetization is excited by a broadband α pulse and phase encoded for time T_p. The gradient shape can be characterized by an amplitude A, gradient ramp time R, and a plateau length P. The repetition time is given by T_R. These parameters, together with the acoustic FRF of the gradient set, determine the mechanical vibration and the accompanying acoustic sound level.

has been modified into so-called multipoint mapping techniques [4,5].

In general, all MRI techniques are inevitably accompanied by acoustic noise generated by the gradient coils. The source of this noise is the rapid switching of currents in the gradient coils, which induce strong Lorentz's forces causing mechanical vibration in the gradient set. As the SPI pulse sequence uses a very short repetition time and relatively high gradient amplitudes, it usually leads to excessive and sometimes even dangerous mechanical vibration of the gradient set, thus limiting the data acquisition speed. One possible approach to avoid the mechanical vibration is the use of gradual gradient switching, which minimizes big gradient jumps between consecutive phase encoding steps. This technique is called SPRITE and is described in [6,7]. SPRITE allows the use of very short repetition times and produces acoustic noise levels comparable to the usual background noise of the MRI room. However, the price to be paid for this "silent" SPI version can be high. For experiments requiring a long acquisition, the mean power deposited into the gradient coils is high, causing gradient overheating. Although, with a modern, water or air-cooled, gradient set this problem can be minimized and SPRITE experiments can be performed [2]. In some MRI systems, however, SPRITE can lead to the overheating of the gradient coils additional delays for cooling have to be included into the experiment to prevent damage to the gradients [8]. One possible way to decrease the heat deposited by SPRITE into the gradient set is to avoid the collection of data in the extremities of k-space, where the encoding gradients reach their maximum. These so-called centric scan SPRITE modification has additional benefits, such as an increase in acquisition speed and an increase of signal to noise ratio (S/N) and T_1 contrast [9].

Recently, several methods to reduce the acoustic noise levels of MRI protocols have been published, e.g., noise cancellation by generating an antiphase acoustic wave [10], optimized gradient shapes [11,13], optimized gradient coil design with active acoustic control [14], and a combinantion of the previous techniques with tailored gradients [15].

In this paper, we investigate the effectiveness of sound attenuation by gradient-shape adjustment as an alternative to the SPRITE method. The idea of using "soft" sinusoidal shaped gradient pulses with a narrow and low frequency bandwidth has been successfully applied to the fast spin echo (RARE) and fast gradient echo (FLASH) sequences [13]. However, it has been reported that the efficiency of this method decreases with a decrease in T_R. We show that based on the frequency response analysis of an imaging gradient system and the frequency characteristics of the gradient program for SPI, there is still room to optimize the gradient shape parameters to substantially reduce mechanical vibration and at the same time prevent overheating of the gradient set, despite the short repetition time which is typically used for SPI.

2. Methods

2.1. Experimental setup

To investigate the effectiveness of the sound pressure level (SPL) attenuation by gradient shape adjustment, three different gradient sets were used: a 72-mm self-shielded gradient system SGRAD 123/72/S (o.d./i.d.) (Magnex, UK) installed in a vertical bore, 11.7 T magnet (Magnex, UK), a 120-mm diameter gradient insert SGRAD 205/120/S (Magnex, UK) and a 305-mm diameter SGRAD MK II 395/305/S (Magnex, UK) installed in a horizontal bore, 7 T magnet (Magnex, UK). Both spectrometers were connected to an Avance DRX Bruker console (Bruker, Karlsruhe, Germany).

Acoustic noise was measured using a Bruel and Kjaer 2238 Mediator sound level meter equipped with a prepolarized free-field condenser microphone type 4188. For all measurements the microphone was centered 20 cm deep into the magnet and connected to the sound meter by a double-shielded cable. For the frequency response function measurements of the gradient sets, the analog output of the sound meter was connected to a digital scope (Tektronix TDS 3032) from which the digitized data were transferred onto a PC and further processed with Matlab software (The MathWorks, Natick, MA). In all acoustic measurements the mean equivalent sound pressure level (SPL) was recorded (as defined by IEC 1672) and the results are shown both in the C and A-mode. The latter takes into account the physiological characteristics of human hearing.

2.2. Frequency response function of the MRI system

It has been shown that the electromechanical structure of the MRI system forms an unit that displays a linear response to the applied gradient pulses [16]. The output from the system, which can be observed as a mechanical vibration accompanied by acoustic frequencies, is given by equation:

$$P(f) = H(f) \cdot G(f), \tag{1}$$

where $H(f)$ is the frequency response function (FRF), which is independent of the system's, input, and $G(f)$ is the frequency spectrum of the gradient pulse sequence. Thus, once the FRF for a spectrometer is known, the acoustic response of this system can be calculated as the product of $G(f)$ and $H(f)$. The FRF usually varies for different scanners, depending on the mechanical construction of the gradient coils and cryostat [17–19]. However, all systems appear to have a significantly reduced response at the lower frequencies [16]. This property can be utilized for the design of quiet pulse sequences if its major components in the frequency profile can be moved into this low frequency area [11]. In practice, the FRF can be measured by the broadband and uniform excitation of the gradient system, e.g., with frequency limited "white" noise from a noise generator [16] with a *sinc*-shaped gradient pulse which has uniform frequency characteristics over the desired frequency range [11] or by sinusoidal sweeps over the measured frequency range [20].

All measurements were performed using a sinc-shaped gradient pulse (vide infra). The FRF of each x, y, and z-gradient channel was calculated separately as the Fourier transform of the acoustic response to a 40-lobe sinc gradient pulse of 10 ms duration, which had a flat spectrum from 0 to 4 kHz [11]. Typical FRFs for all of three gradient sets are shown in Fig. 2. Note that all of the FRFs exhibited a reduced response for frequencies below ~600–800 Hz with the exception of the 11.7 T z-gradient, which did not show a reduced response in this frequency region. On the other hand, the SPL produced by this z-gradient was about 18 dB lower (C-mode) compared to the remaining transverse gradient channels of the same system and therefore its contribution to the total SPL could be considered negligible. Moreover, both small diameter gradient sets showed a further partial reduction of the acoustic response for higher frequencies; for the 120-mm gradient this partial reduction can be observed up to 1.7 kHz and for the 72-mm gradient for even higher frequencies, up to 2 kHz.

2.3. Frequency spectrum of the SPI gradient program

The SPI gradient pulse program is relatively simple and one period can be fully characterized by: gradient amplitude A, plateau length P, ramp time R, ramp shape, and a repetition time T_R as shown in Fig. 1. Assuming for the moment that the applied phase encoding is an even and periodical function (i.e., neglecting the

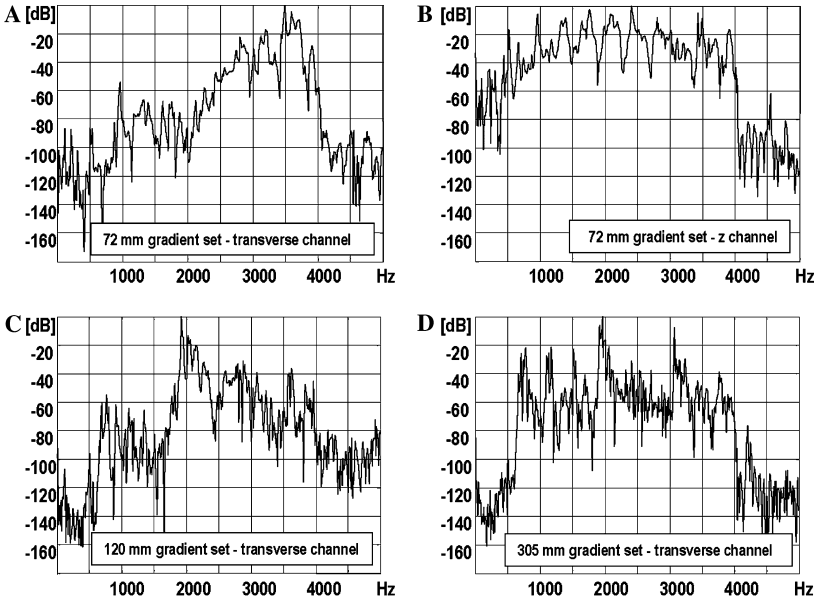

Fig. 2. Typical acoustic FRF for all three examined gradient sets: (A) 72 mm gradient coil (11.7 T spectrometer) for the transverse channel, (B) longitudinal-channel of the same gradient set, (C) 120 mm gradient insert (7 T spectrometer) for the transverse channel, and (D) 305 mm main gradient system (7 T spectrometer) for the transverse channel. The FRFs were measured in the range of 0–4 kHz; magnitudes were rescaled to 1 (a.u.) and are shown as $10 \log H^2(f)$ for each gradient. All measured FRFs exhibited reduced response for low frequencies except the 72 mm z-gradient. The FRF for this gradient selects certain low frequencies, however, the overall acoustic level was about 18 dB below both the transverse gradient channels of the same system. Note that both small gradient sets showed partial response reduction for higher frequencies. For the 120-mm gradient this partial reduction can be observed up to 1.7 kHz and for the 72 mm inset even up to 2 kHz.

amplitude changes between successive phase encoding steps), the gradient time course $G(t)$ can be represented by a Fourier series [21]

$$G(t) = \frac{a_0}{2} + \sum_{n=1}^{\infty} a_n \cos\left(n\frac{2\pi}{T_R}t\right), \quad \text{where}$$
$$a_n = \frac{2}{T_R}\int_0^{T_R} G(t)\cos\left(n\frac{2\pi}{T_R}t\right)\mathrm{d}t \quad \text{for } n = 0, 1, 2, \ldots \tag{2}$$

Now consider two types of gradient shapes: a gradient pulse with a linear ramp and a gradient with a sinusoidal ramp, as has been proposed by Hennel et al. [11–13]. The latter has been found useful for the minimization of acoustic noise in fast MRI sequences. Calculating the coefficients a_n for the non-zero frequencies (i.e., $n=1, 2, \ldots$), we obtain for the linear ramped gradient:

$$a_n = \frac{A(-1)^n}{\pi^2 n^2}\left(\frac{R}{T_R}\right)^{-1}\left[\cos\left(n\pi\frac{P}{T_R}\right) - \cos\left(n\pi\left(\frac{P}{T_R}+\frac{2R}{T_R}\right)\right)\right]. \tag{3}$$

and for gradient pulse with the sinusoidal slopes:

$$a_n = \frac{A(-1)^n}{\pi n}\left(1-4n^2\left(\frac{R}{T_R}\right)^2\right)^{-1}\left[\sin\left(n\pi\frac{P}{T_R}\right) + \sin\left(n\pi\left(\frac{P}{T_R}+\frac{2R}{T_R}\right)\right)\right]. \tag{4}$$

The position of each spectral line a_n on the frequency axis is given by $f_n = \frac{n}{T_R}$. The dependency of spectral power for a gradient pulse with linear slope on the parameters R/T_R and P/T_R is shown in Fig. 3. As seen from the plot, the power of the fundamental frequency is relatively insensitive to changes in R/T_R and decreases only for very low ratios. For the higher frequencies the total power declines with increasing R/T_R. The conclusion from these observations is that the only possible way to minimize the power level of acoustic noise is to position the fundamental frequency into the low amplitude range of the FRF and to choose a sufficiently long R and P. Thus, for minimization of acoustic noise by gradient timing, the following condition must be satisfied:

$$T_R > \frac{1}{f_r}, \tag{5}$$

where f_r is the upper limit of the flat reducing part of FRF.

When calculating the ratio of the mean power deposition into the gradient sets for a SPI with linear slope gradient and the SPRITE sequence, both using the same repetition time T_R, we obtain:

$$\frac{P_{\text{linear slope}}}{P_{\text{SPRITE}}} = \frac{\int_0^{T_R} I_{LS}^2(t)\,\mathrm{d}t}{\int_0^{T_R} I_{\text{SPRITE}}^2(t)\,\mathrm{d}t} = \frac{0.667\cdot R + P}{T_R} \tag{6}$$

and for the sinusoidal gradient slope:

$$\frac{P_{\text{sinusoidal slope}}}{P_{\text{SPRITE}}} = \frac{\int_0^{T_R} I_{SS}^2(t)\,\mathrm{d}t}{\int_0^{T_R} I_{\text{SPRITE}}^2(t)\,\mathrm{d}t} = \frac{0.625\cdot R + P}{T_R}, \tag{7}$$

where $I_{LS}(t)$ and $I_{SS}(t)$ represent the instantaneous gradient current for linear or sinusoidal slope gradients, respectively.

Note, employing longer gradient ramps increases the gradient duty cycle when comparing to the analogous standard SPI method with abrupt gradient. Consider, for example, the original SPI with as gradient plateau of the length $P=0.1\cdot T_R$ and a gradient ramp $R=0.1\cdot T_R$. If the maximum available slope with duration $R=0.45\cdot T_R$ is used, the increase in power deposited into the gradient coils amounts to a factor of 2.4 for a linear and a factor of 2.29 for a sinusoidal shaped gradient ramp. On the another hand, when comparing the modified sequence to the SPRITE sequence, both using the same T_R, the deposit power is less by a factor of 2.5 for the linear and a factor of 2.6 for the sinusoidal shaped gradient.

3. Results and discussion

The SPI sequence with adjustable gradient plateau and ramp length, together with adjustable gradient ramp shape was implemented on both spectrometers. To inves-

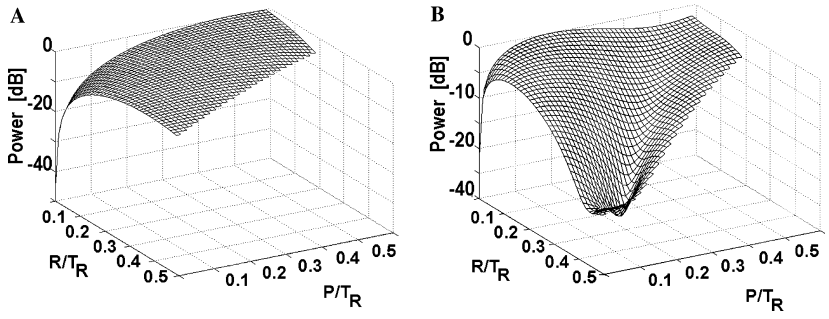

Fig. 3. SPL simulations for a gradient pulse with linear gradient ramp as a function of R/T_R and P/T_R: (A) power for the fundamental frequency (i.e., $n=1$) and (B) the power for the frequencies in the range $n=(2\text{–}99)$, calculated as $P = 10\log\sum(a_n^2)$. The total power for the upper frequencies decreases as R increases and the minimum is reached around $R/T_R=0.35$ and $P/T_R=0.15$.

tigate the influence of the gradient pulse parameters on the SPL, two different types of experiments were performed: SPL as a function of the gradient slope length and/or shape (linear versus sinusoidal) and changes in SPL as a function of the time repetition between experiments. All experiments were performed with the following gradient amplitudes: 150 mT/m for the 72 mm gradient system, 93 mT/m for the 120 mm gradient system, and 25 mT/m for the 305 mm gradient system. The plateau length of $P = 0.4$ ms was kept the same for all experiments. Fig. 4 shows the results from these measurements. In the first set of experiments SPL was measured for both types of gradient slopes (linear and sinusoidal) and their lengths changed up to the maximum length of $R = 1.6$ ms, while the repetition time was kept constant at $T_R = 4$ ms. It can be seen that the best acoustic noise suppression was achieved for the 72 mm gradient system where replacing the 175 μs linear ramp by the 1.6 ms sinusoidal slope resulted in a 23.2 dB decrease of acoustic noise (measured in A-scale). This measured SPL was only 4 dB above the background noise in the room. The power deposition into the gradient system dropped down by a factor of 3 when compared to the SPRITE sequence. Similar results were obtained for the 120 mm gradient system where 20.5 dB (A-scale) suppression of the noise level was achieved for a 1.6 ms slope length. Again, this was about 4 dB above the background noise. The least effective acoustic noise suppression was observed for the 305 mm gradient system, where only a 12 dB reduction of acoustic noise was achieved. This was about 30 dB (A-scale) above the background noise level. When the longer repetition time $T_R = 8$ ms was used and a longer gradient slope of $R = 3.6$ ms could be used, the SPL magnitude dropped by 19.8 dB (A-scale) but was still about 10 dB above background level.

Measurement of acoustic noise level variation as a function of T_R was done from $T_R = 3$–12 ms with a 1 ms step increment and a constant gradient slope $R = 1.2$ ms. The obtained values are shown in Fig. 4 (right column) and reveal that no substantial variations of SPL (less than ±2.5 dB for both the 72 and the 120 mm gradient system) with changing repetition time occurred.

To explain the different performances of acoustic noise suppression when comparing the small versus the big

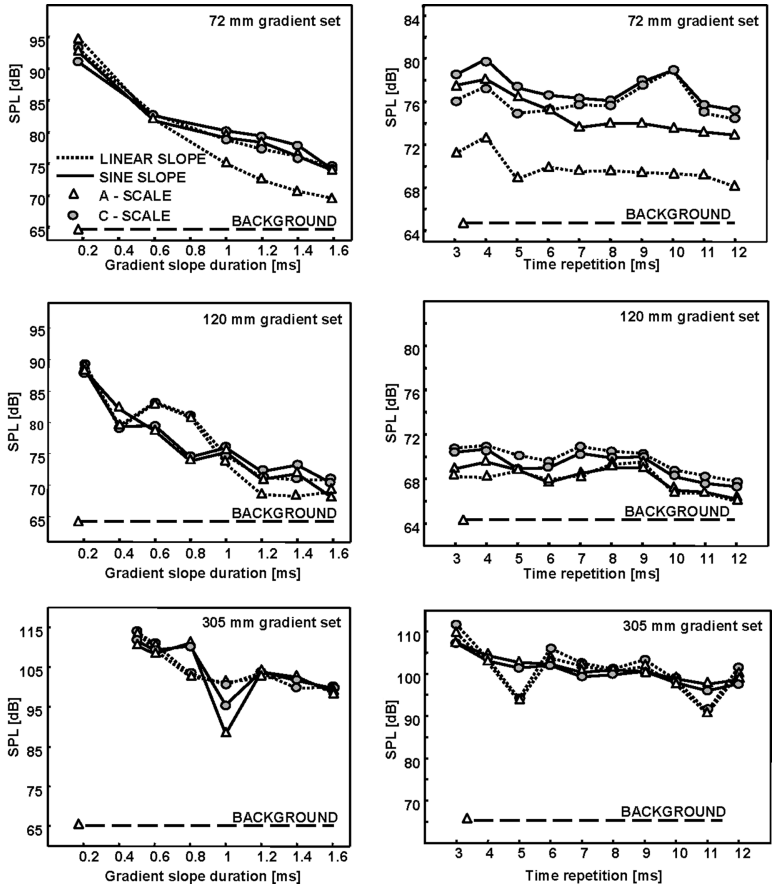

Fig. 4. Results of the acoustic noise level measurements for the SPI sequence using three different types of the gradient sets: a 72, a 120, and a 305 mm set. The influence of the gradient slope duration on the final SPL is shown in the left-hand column, the dependence on the sequence repetition rate is shown in the right-hand column. For each measurement two types of gradient slopes were compared: the linear and the sinusoidal. The best performance of acoustic noise suppression (>20 dB) was achieved for the 72 and the 120 mm gradient sets. The SPL reduction for the 305 mm gradient set was only about 12 dB, this is explained by the shape of the FRF (see text).

gradient set, SPI sound profiles were recorded and frequency spectra calculated [19]. The results are shown in Fig. 5. It can be seen that for both smaller gradient sets the main spectral lines are shifted towards higher frequencies, while in the case of the 305 mm gradient set, most of the acoustic energy is concentrated around 750 Hz. The relative contribution of the individual frequencies to the final SPL of the acoustic suppressed sequence can be shown on the cumulative histogram defined as:

$$P(n) = 10\log_{10}\sum_{i=1}^{n}\frac{(a_i^2)_{\text{acoustic suppression}}}{\sum_{j=1}^{N}(a_j^2)_{\text{without acousticm supression}}}, \qquad (8)$$

i.e., the cumulative histogram is normalized to the acoustic noise power generated by the gradients using a linear slope. Fig. 5D shows the comparison of the acoustic noise suppression performance for the 72 and the 305 mm gradient systems. The cumulative histograms were calculated for a gradient sequence using a sinusoidal gradient slope, $R = 1.6$ ms and $T_R = 4$ ms. It can be seen that for the larger bore gradient system the contribution of the third harmonic to the overall acoustic sound power is 24 dB. This explains the bad performance for acoustic noise suppression on the 305 mm gradient system.

The overall image quality is not affected by the changes to reduce the acoustic noise reduction. Fig. 6 shows a 3D reconstructed image of a jujube candy, characterized by relaxation times $T_1 = 950$ ms, $T_2^* = 270$ μs, obtained with silent SPI sequence on the 11.7 T spectrometer using the following parameters: FOV = 5 × 5 × 2.5 cm, resolution 128 × 128 × 32 points, 5.3° α pulse, $T_p = 300$ μs, gradient plateau $P = 400$ μs, sinusoidal gradient slope length of $R = 1.6$ ms and time repetition $T_R = 4$ ms, one average and a total acquisition time of 35 min. The mean equivalent SPL over the whole experiment was 73.6 dB and the maximum SPL value was detected as 78.5 dB. For comparison the same experiment using linear gradient slopes with default length of $R = 175$ μs resulted in the mean SPL of 95.6 and 100.1 dB peak level. When comparing SPI using a sinusoidal gradient slope with experiments performed using the default linear ramp, an increase of the gradient power deposition by a factor of 2.71 in each repetition cycle can be observed. The same comparison between the sinusoidal gradient SPI and the analogous experiment performed with standard rectilinear SPRITE reveals that the optimized gradients deposit 2.85 times less power as compared to SPRITE.

4. Conclusion

We have presented a modified SPI sequence employing optimized gradient parameters to minimize acoustic vibration in the MRI scanner. It has been shown that using longer ramp and/or shaped gradient slopes can significantly reduce acoustic noise, even for SPI sequences using relatively short repetition times on the order of a few milliseconds. This is because the frequency response

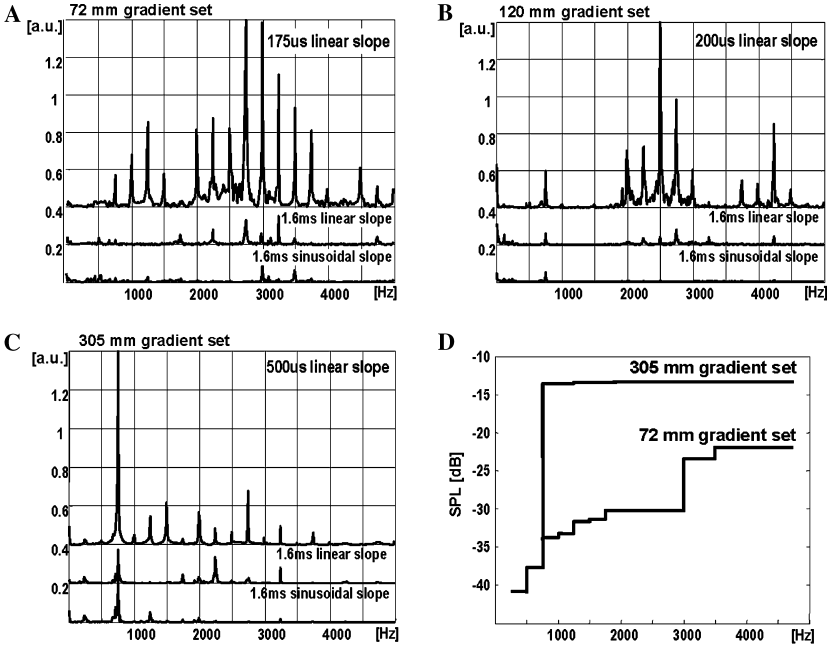

Fig. 5. SPI sequence acoustic spectra obtained with different gradient slope length and shapes (spectra for the same system are plotted shifted up 20 and 40% for clarity): (A) 72 mm gradient system, (B) 120 mm gradient system, and (C) 305 mm gradient system. Note, that for both small gradient sets (A) and (C) the acoustic spectrum is a composite of many spectral lines shifted towards to the higher frequencies. These frequencies can be significantly suppressed by selecting longer gradient slopes. For the 305 mm system one major frequency occurs at 750 Hz. The cumulative histogram (D) shows the huge ~24 dB contribution of this frequency to the acoustic noise level, even after using 1.6 ms sinusoidal gradients slope.

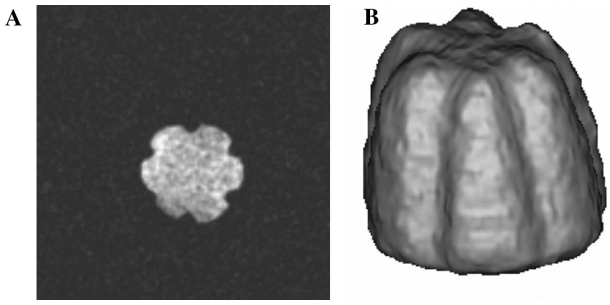

Fig. 6. (A) A 2D slice from 3D ($128 \times 128 \times 32$) image with $S/N = 10.5$ and (B) surface rendered 3D image of a jujube candy obtained with SPI using sinusoidal modulated gradients. The average noise level during the experiment was 73.6 dB and peak noise level 78.5 dB (both measured in A-mode), while the background noise level in the room was about 65 dB. This was more than 20 dB less as obtained with linear gradient slopes with default length of $R = 175\,\mu s$.

function of typical small-bore gradient coils has an extended reduced response area at the low frequency range compared to the larger bore systems.

However, effective SPL suppression requires the use of gradient ramp lengths of more than 1 ms, which sets a limit for the minimum T_R around 3 ms. On the other hand, ramping of the gradients provides benefits in the form of a reduction in the instantaneous power deposition into the gradient coils as compared to SPRITE gradient switching. Even if the optimized gradients shape reduces gradient coil heating, problems can still occur at the extremities of k-space where the absolute magnitude of the gradients is highest. An elegant approach to minimize this problem is centric scans sampling of k-space [9]. Also, a combination of both methods, i.e., usage of optimized gradient switching together with centric scan sampling, could provide a further gradient power reduction if a slightly longer repetition time is not an obstacle.

The results proved that SPI, with optimized gradient parameters, could be an excellent alternative to the SPRITE method, especially when overheating of gradients might be a concern. On the other hand, even if optimized gradients contribute to the lowering of heat deposition as compared to the SPRITE method, the SPI method is gradient intensive and should never be run without actively cooled and monitored gradients. However, using careful considerations, exceptions are possible [8].

The implementation of the method is very simple especially for systems where the shape of the gradient slope can be altered or the duration of the ramp time can be adjusted.

Acknowledgment

We thank IMRIS Inc. (Winnipeg, MB) for the use of their sound level meter.

References

[1] S. Emid, J.H.N. Creyghton, High resolution NMR imaging in solids, Phys. B 128 (1985) 81.
[2] C.B. Kennedy, B.J. Balcom, I.V. Mastikhin, Three-dimensional magnetic resonance imaging of rigid polymeric materials using single-point ramped imaging with T_1 enhancement (SPRITE), Can. J. Chem 76 (1998) 1753–1765.
[3] P. Bendel, M. Davis, E. Berman, G.W. Kabalka, A method for imaging nuclei with short T_2 relaxation and its application to Boron-11 NMR imaging of a BNCT agent in an intact rat, J. Magn. Reson. 88 (1990) 369–375.
[4] Z.H Cho, Y.M. Ro, Multipoint k-space point mapping (KPM) technique for NMR microscopy, Magn. Reson. Med. 32 (1994) 258–262.
[5] M.A. Fernández-Seara, S.L. Wehrli, F.W. Wehrli, Multipoint mapping for imaging of semi-solid materials, J. Magn. Reson. 160 (2003) 144–150.
[6] B.J. Balcom, R.P. MacGregor, S.D. Beyea, D.P. Green, R.L. Armstrong, T.W. Bremner, Single-point ramped imaging with T_1 enhancement (SPRITE), J. Magn. Reson. A 123 (1996) 131–134.
[7] I.V. Mastikhin, B.J. Balcom, P.J. Prado, C.B. Kennedy, SPRITE MRI with prepared magnetization and centric k-space sampling, J. Magn. Reson. 136 (1999) 159–168.
[8] S.D. Beyea, S.A. Altobelli, L.A. Mondy, Chemically selective NMR imaging of a 3-component (solid–solid–liquid) sedimenting system, J. Magn. Reson. 161 (2003) 198–203.
[9] M. Halse, D.J. Goodyear, B. MacMillan, P. Szomolanyi, D. Matheson, B.J. Balcom, Centric scan SPRITE magnetic resonance imaging, J. Magn. Reson. 165 (2003) 219–229.
[10] M. McJury, R.W. Stewart, D. Crawford, E. Toma, The use of active noise control (ANC) to reduce acoustic noise generated during MRI scanning: some initial results, Magn. Reson. Imaging 15 (1997) 319–322.
[11] F. Hennel, F. Girard, T. Loenneker, "Silent" MRI with soft gradient pulses, Magn. Reson. Med. 42 (1999) 6–10.
[12] F. Girard, V.L. Marcar, F. Hennel, E. Martin, Anatomic MR images obtained with silent sequences, Radiology 216 (2000) 900–902.
[13] F. Hennel, Fast spin echo and fast gradient echo MRI with low acoustic noise, J. Magn. Reson. Imaging 13 (2001) 960–966.
[14] P. Mansfield, B. Haywood, Principles of active acoustic control in gradient coil design, MAGMA 10 (2000) 147–151.
[15] B.L.W. Chapman, B. Haywood, P. Mansfield, Optimized gradient pulse for use with EPI employing active acoustic control, Magn. Reson. Med. 50 (2003) 931–935.
[16] R.A. Hedeen, W.A. Edelstein, Characterization and prediction of gradient acoustic noise in MR imagers, Magn. Reson. Med. 37 (1997) 7–10.
[17] P. Mansfield, B.L.W. Chapman, R. Bowtell, P. Glover, R. Coxon, P.R. Harvey, Active acoustic screening: reduction of noise in gradient coils by Lorentz force balancing, Magn. Reson. Med. 33 (1995) 276–281.
[18] R.W. Bowtell, P. Mansfield, Quiet transverse gradient coils: Lorentz force balanced designs using geometrical similitude, Magn. Reson. Med. 34 (1995) 494–497.
[19] Z.H. Cho, S.H. Park, J.H. Kim, S.C. Chung, S.T. Chung, J.Y. Chung, C.W. Moon, J.H. Yi, C.H. Sin, E.K. Wong, Analysis of acoustic noise in MRI, Magn. Reson. Imaging 15 (1997) 815–822.
[20] W. Li, C.K. Mechefske, C. Gazdzinski, B.K. Rutt, The spatial distribution and prediction of gradient induced acoustic noise in a 4T MRI scanner, in: Proceedings of the 11th Annual Meeting of ISMRM, Toronto, 2003, p. 746.
[21] J.J. Tuma, R.A. Walsh, Engineering Mathematics Handbook, McGraw-Hill, NewYork, 1997 pp. 163–176.